Study of the local distortions of the perovskite system $La_{1-x}Sr_xCoO_3$ ($0 \leq x \leq 0.35$) using the extended x-ray absorption fine structure technique

Y. Jiang,[1] F. Bridges,[1] N. Sundaram,[1] D. P. Belanger,[1] I. E. Anderson,[1] J. F. Mitchell,[2] and H. Zheng[2]
[1]*Physics Department, University of California, Santa Cruz, California 95064, USA*
[2]*Materials Science Division, Argonne National Laboratory, 9700 Cass Avenue, Argonne, Illinois 60439, USA*
(Received 1 June 2009; revised manuscript received 8 September 2009; published 26 October 2009)

We present a temperature-dependent extended x-ray absorption fine structure (EXAFS)/x-ray absorption near edge structure (XANES) investigation of $La_{1-x}Sr_xCoO_3$ (LSCO) over a wide doping concentration range ($0 \leq x \leq 0.35$). Five of the samples are nanoparticles ($x=0.15$, 0.20, 0.25, 0.30, and 0.35) and four are bulk powders ($x=0$, 0.15, 0.20, and 0.30). From the EXAFS analysis, we find that the Co-O bonds are well ordered for both bulk and nanoparticle materials and there is no clear evidence for a Jahn-Teller (JT) distortion in the LSCO system (either static or dynamic). The distortion of the Co-O bond with increasing T, parameterized by the width of the pair distribution function (PDF), $\sigma(T)$, can easily be modeled using a correlated Debye model with a high correlated Debye temperature ~800 K. There is also no evidence for a step in plots of σ^2 vs T. In addition, the very small nonthermal contribution to σ^2 for the Co-O (PDF), σ^2_{static}, sets an upper limit on the extent of any Jahn-Teller distortion at low T. These experiments are inconsistent with the existence of a significant fraction of Co sites with an intermediate spin (IS) state, for which there is a JT active e_g electron on the Co atoms. We cannot, however, exclude the possibility of a tiny fraction of sites having a JT distortion or some other (non-JT active) means of producing an IS state. The bulk samples are well ordered out to at least the third neighbors (Co-Co) while the nanoparticles show increased disorder and a reduction in coordination for Co-Co. XANES data are also presented, and, for both bulk and nanoparticle samples, there is essentially no edge shift with increasing Sr concentration. Bond-valence sums also indicate no change in effective Co valence. These results indicate that when holes are introduced via Sr doping, they have little Co($3d$) character and the Co configuration remains close to $3d^6$; we argue that the holes have mostly O($2p$) character and are localized more on the O sites.

DOI: 10.1103/PhysRevB.80.144423 PACS number(s): 71.70.Ej, 61.05.cj

I. INTRODUCTION

$LaCoO_3$ (LCO) and Sr-doped $La_{1-x}Sr_xCoO_3$ (LSCO) belong to a family of perovskites that exhibits many interesting properties [such as magnetization and colossal magnetoresistance (CMR)] that have been studied extensively.[1] Though the perovskite system $La_{1-x}Sr_xCoO_3$ has not received as much attention as other perovskite CMR materials, such as $La_{1-x}A_xMnO_3$ (A=Ca, Sr, etc.), it has generated interest over the past decades due to its rich but puzzling phase diagram.[1–4] The LSCO system has a spin-cluster-glass insulator to ferromagnetic metal transition when the Sr concentration x exceeds ≈0.18.[2,5–8] Increasing the temperature will invoke a spin-glass insulator to paramagnetic insulator transition or FM metal to paramagnetic metal transition depending on the Sr concentration.

However, to date, the many studies of the perovskite system $La_{1-x}Sr_xCoO_3$ have not solved a long-standing controversy regarding the ordering of the Co spins (specifically the Co spin configuration) and the ferromagnetic transition; the spin order depends strongly on the competition between the exchange interaction, E_{ex}, [which includes the Hubbard U parameter and the (Hund's rule) interaction J_H; $E_{\text{ex}} \sim U - J_H$] and the crystal-field splitting energy, $\Delta E = 10Dq$. When these energies are comparable as in the cobaltite systems, small changes in energy can change the occupied spin states.

As is well-known for $LaCoO_3$ at $T \sim 0$, the ground state of nonmagnetic (weakly diamagnetic) Co^{3+} is a low spin state ($S=0$) for which the six $3d$ electrons in the t_{2g} state are aligned antiparallel ($10Dq > E_{\text{ex}}$). With increasing temperature, the low spin (LS) configuration of $LaCoO_3$ changes to a higher-spin magnetic configuration. Some investigators[9–21] propose that a partial transition to an intermediate spin (IS) state ($S=1$) occurs, with five d electrons in the t_{2g} state and one in an e_g state. In this case, the single e_g electron on Co should be Jahn-Teller (JT) active and lead to a splitting of the Co-O bond lengths about Co. Others suggest that the transition is to a mixture of the LS and high spin (HS)[22–29] states where the HS state has four d electrons in the t_{2g} state and two in the e_g, with $S=2$ as a result of Hund's rule coupling. A mixture of these two models is also presented as a possibility.

In addition to temperature inducing a spin state transition in $LaCoO_3$, the addition of Sr also affects the spin state. With an increasing Sr concentration, some Co^{4+} ions might be expected in the LSCO system, under the formal assumption that O carries a −2 charge; then the formal valence of Co is $3+x$, a mixture of 3+ and 4+. Assuming the five remaining $3d$ electrons are in the t_{2g} state on some sites (starting with a LS configuration), the spin of Co^{4+} would be $S=1/2$, and not JT active. Similarly for the HS configuration with $E_{\text{ex}} \gg 10Dq$; the highest occupied electron state is again a t_{2g} state and this configuration is also not JT active. For $E_{\text{ex}} \sim 10Dq$ as appears to be the case here, the situation is more complex.

If, instead, the added holes are primarily localized on the O $2p$ sites, the Co $3d$ character, and hence the *effective* Co valence, might change relatively little. Note that because of significant covalency in the transition-metal oxides, this ionic picture is only a rough approximation. Many

calculations—see, for example, the recent work in Refs. 21 and 30—show this covalency as an increase in the occupation of the $3d$ states; i.e., for Co in $LaCoO_3$, a $3d$ occupation larger than 6, with some fractional occupation of the e_g states (for the LS configuration).

Of the various spin states for $LaCoO_3$, only an intermediate spin state ($S=1$), with one e_g electron, is expected to be strongly Jahn-Teller active, as observed for example, in extensive studies of the manganites.[31–33] Such a Jahn-Teller distortion about the Co atom would lower the symmetry, leading to four shorter Co-O bonds and two longer bonds. Consequently, the presence of a distortion of the Co-O distribution function has been considered a signature for the IS state. However, the theoretical studies cited above generally use the $R\bar{3}c$ space group for the lattice and thus exclude energy splittings arising from a JT distortion. In addition, a recent theoretical study by Pandey *et al.*[21] indicates that spin-orbit coupling also splits the e_g degeneracy without a JT distortion; if such a splitting is sufficient, then an intermediate state might be achieved without a JT distortion. Finally, a JT distortion would not be observed if the e_g electrons were hopping much faster than phonon frequencies and the O atoms were at some average position between the Co atoms (as occurs for CMR manganites in the ferromagnetic state at low T).[31,32]

A number of experiments, including neutron pair distribution function (PDF), x-ray diffraction, x-ray photoelectron spectroscopy (XPS), and x-ray absorption fine structure (XAFS), have been done on $La_{1-x}Sr_xCoO_3$ bulk material and lead to conflicting results. In particular, early neutron PDF results[34] suggested a significant fraction of Co have a large distortion of the Co-O bond in the distribution function, but other recent experiments show no direct evidence of the IS state.[26,27,29] In our recent study of the Co-O pair in bulk materials using both extended x-ray absorption fine structure (EXAFS) and neutron PDF analysis, no evidence of a JT distortion was observed.[35]

Because of the sensitivity of the Co spin state to rather small changes in the structure, these states, and the magnetism of $La_{1-x}Sr_xCoO_3$, might also be sensitive to small structural changes that usually accompany the reduction in particle size to the nanoscale; however, to date no experiments on the local structure of nanoparticle $La_{1-x}Sr_xCoO_3$ have been carried out.

To better understand the spin state transition induced by temperature and Sr concentration in the LSCO system, we have applied the EXAFS technique to bulk and nanoparticle $La_{1-x}Sr_xCoO_3$ powders ($0 \leq x \leq 0.35$) and analyzed the data for the further-neighbor pairs, out to the Co-Co pair. This range of Sr concentration spans the transition of the spin-glass insulator to the ferromagnetic metal in bulk material.[1–4] EXAFS is a very powerful technique for investigating the local structure about a central atom—here the Co ion. Because of the previously reported[14,16] positive results for a JT distortion, new neutron PDF experiments have also been carried out on most of the same bulk and nanoparticle samples; part of our neutron PDF results for bulk samples have been published,[35] and a detailed study for both bulk and nanosamples is in preparation.[36] The EXAFS and new neutron PDF results agree—for these samples there is little evidence of a significant fraction of Co sites with a JT distorted Co-O bonds (at most 10%), or any unusual distortion of the lattice out to at least the third neighbors.

TABLE I. Sample details for the nanoparticle and bulk samples. In the table, *B* means bulk sample, *N* means nanoparticle sample, and *X* means the date that data were collected for experiment no. 1 (June 2006) and experiment no. 2 (July 2007). MZ stands for Mitchell and Zheng and S stands for Sundaram, while SA stands for Sundaram and Anderson.

Concentration (type)	June 2006	July 2007	Sample maker
0 (*B*)		*X*	MZ
0.15(*N*)	*X*	*X*	SA
0.15(*B*)		*X*	S
0.20(*N*)		*X*	SA
0.20(*B*)		*X*	S
0.20(*B*)	*X*	*X*	MZ
0.25(*N*)	*X*	*X*	SA
0.30(*N*)		*X*	SA
0.30(*B*)	*X*	*X*	MZ
0.35(*N*)	*X*	*X*	SA

This article is organized as follows: first, we briefly describe the EXAFS technique and provide experiment details in Sec. II; next, we present the x-ray absorption near edge structure (XANES) data in Sec. III A and an EXAFS data analysis in Sec. III C. Then, we discuss our EXAFS fit results for both the shortest Co-O bonds and longer bonds in Sec. III D. Finally, we provide a brief summary of the results in Sec. IV.

II. EXPERIMENTAL DETAILS AND EXAFS TECHNIQUE

Transmission EXAFS data at the Co *K* edge were collected on beam line 10-2 at the Stanford Synchrotron Radiation Lightsource (SSRL), over a wide temperature range (4–320K) for both powdered and nanoparticle samples. For high energy resolution, we used a double Si(111) monochromator, with a slit size of 0.5 mm $\times$ 10 mm for each experimental run, giving an energy resolution (δE) of 1.2 eV that is comparable to the Co core-hole lifetime broadening $\approx$1.46 eV. To reduce the harmonic content in the x-ray beam, we detuned the monochromator crystals 50% at 7900 eV. Finally, for the XANES investigation, we used a small energy step (0.35 eV) through the edge region, and also collected simultaneous data on a reference Co foil to correct for any tiny drifts of the monochromator system.

To investigate the effect of particle size, we collected data on both nanoparticle (10–50 nm) and powdered bulk samples ($\leq$5 μm). Details about the samples are provided in Table I. To prepare EXAFS samples, bulk material was first ground using a mortar and pestle; the fine powder was then passed through a 400-mesh sieve and brushed onto adhesive tape. The tape preferentially holds the smaller grains ($\leq$5 μm) in a thin layer; two pieces of tape were pressed together (double

layer) to encapsulate the powder. Two double layers were used for the EXAFS measurements at the Co *K* edge, which gives an absorption step height of 0.5. For the nanoparticles, the powder was also brushed onto tape, but due to the small particle size (10–50 nm), eight double layers of tape were required to give a step height of 0.3. To vary the temperature, the EXAFS samples were mounted in an Oxford Helium cryostat with the samples oriented perpendicular to the x-ray beam.

Details about the sample preparation for the bulk material were given previously.[35] $La_{1-x}Sr_xCoO_3$ nanoparticles ($x=0.15$, 0.20, 0.25, 0.30, and 0.35) were synthesized using the amorphous heteronuclear complex Diethylenetriaminepentaacetic acid (DTPA) as a precursor. First, a NaOH solution at 1.0 mol/l concentration was added by drops to a mixture solution of $La(NO_3)_3$, $SrNO_3$, and $Co(NO_3)_3$ to prepare the fresh hydroxides. Then, equimolar amounts of DTPA were added to these fresh hydroxides in water to synthesize the complex precursor. The mixture was stirred as it was heated to 80 °C. The transparent solution formed was vaporized slowly at room temperature until a piece of transparent glasslike gel was formed. This precursor was decomposed in air at 300 °C for about an hour to burn off the organic components. The collapsed gel was then heated at 600, 620, 700, or 750 °C for four hours (calcination). While heating at 600 °C resulted in impurities in the x-ray diffraction pattern, calcination at temperatures above 620 °C resulted in sharper x-ray peaks with no impurities, and the peaks became sharper as the calcination temperature increased, which indicates sintering and aggregation of the particles. Hence, 620 °C was considered to be the optimum calcination temperature to obtain the pure nanocrystalline $La_{1-x}Sr_xCoO_3$ phase with the smallest particle size. The oxygen stoichiometry of all the samples was determined by using iodometric titrations.

X-ray diffraction measurements confirmed the formation of pure phase material, and the crystallite sizes, distribution, and structural morphology were determined using bright field imaging techniques and selected area diffraction patterns using the high-resolution FEI Techai 12 Transmission Electron Microscope at University of California, Berkeley and the JEOL 1230 TEM at the University of California, Santa Cruz. Under the calcination temperature of 620 °C, the particle sizes of the nanoparticles range from approximately 10 to 50 nm. Higher calcination temperature causes further aggregation of particles, hence only the powders with a calcination temperature of 620 °C were used in this EXAFS study.

Fits of the EXAFS data were carried out in *r* space to the real, Re, and imaginary, Im, parts of the Fourier Transform (FT) of $k\chi(k)$, using the EXAFS equation for $k\chi(k)$, given by

$$k\chi(k) = \sum_i k\chi_i(k) = \mathrm{Im}\sum_i A_i \int_0^\infty F_i(k,r)\frac{g_i(r_{0i},r)e^{i[2kr+2\delta_c(k)+\delta_i(k)]}}{r^2}dr \quad (1)$$

$$A_i = N_i S_0^2, \quad (2)$$

where $g_i(r_{0i},r)$ is the i^{th} shell, pair distribution function for atoms at a distance r_{0i} from the center atom (here Co), $F_i(k,r)$ is the back scattering amplitude, and $\delta_c(k)$ and $\delta_i(k)$ are the phase shifts from the central and backscattering atom potentials, respectively. The amplitude, A_i, is the product of the coordination number, N_i, from diffraction results and S_0^2, the amplitude reduction factor, which is included to correct for multielectron effects since multielectron processes contribute to the edge step-height but not to the EXAFS amplitude. Experimentally, S_0^2 also corrects for several other small effects. Finally an additional parameter, ΔE_0, describes the difference in edge energy between the value defined for the data (at half height) and the theoretical functions (for which $k=0$ at E_0).

In fitting the EXAFS data, we assume a Gaussian PDF with a width σ for each peak in *r* space; the first few two-path peaks correspond to the Co-O, Co-La/Sr, and Co-Co shells. Also note, that for a given shell, different contributions to σ^2 add up in quadrature if the different distortion mechanisms are uncorrelated; i.e., the time average of $\langle \delta x_{A-\text{static}} \delta x_{B-\text{phonon}} \rangle = 0$ where $\delta x_{A-\text{static}}$ is the static component to the displacement of atom A and $\delta x_{B-\text{phonon}}$ is the instantaneous displacement component of atom *B* from phonons. If Jahn-Teller distortions are present, $\sigma^2_{\text{total}} = \sigma^2_{\text{static}} + \sigma^2_{\text{phonons}} + \sigma^2_{\text{JT}}$ for the Co-O peak. Correlated atomic motions are present for thermal vibrations and are included in models for $\sigma^2_{\text{phonons}}$.

III. EXAFS/XANES DATA REDUCTION AND ANALYSIS

The EXAFS data were reduced using the RSXAP package,[37] which implements standard data reduction techniques. First, a pre-edge background was removed from the data (the Victoreen formula was used to adjust the slope above the edge during the pre-edge subtraction) and an experimental E_0 was defined as the energy of the half-height point on the Co *K* edge. The normalized Co *K* edge data were used for the XANES discussion in the following section. To extract the EXAFS oscillations, a postedge background was removed using a spline with five knots to approximate μ_0 in $\mu(E)=\mu_0[1+\chi(E)]$. The background-subtracted data $\chi(E)$ were then transformed to *k* space $[\chi(k)]$ using the relation $k=\sqrt{\frac{2m(E-E_0)}{\hbar^2}}$.

A. XANES

The final step in the XANES data reduction was to correct for any tiny shifts in the monochromator from one scan to another, using the reference Co foil data collected simultaneously. The position of the first inflection point on the Co foil *K* edge data was set at 7709 eV and each LSCO scan was shifted slightly so that the corresponding Co reference foil data all overlapped within 0.03 eV (all the reference edges were fit to a fiducial scan to determine the relative shifts).

Examples of the Co *K* edges for the bulk and nanoparticle samples are shown in Figs. 1(a) and 1(b). The most striking aspect of these data is that there is very little shift in the edge as the Sr concentration varies from 0 to 35%; the very tiny *K*-edge shift we observe with increasing Sr concentration (Fig. 1) is only 0.15 eV at 30% Sr. In addition, we also find

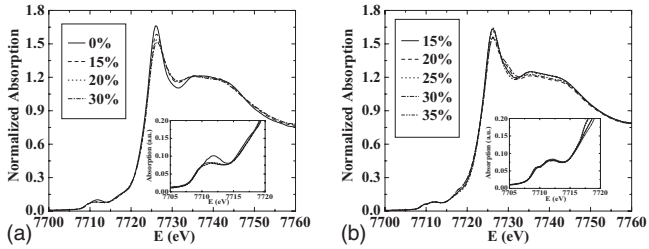

FIG. 1. (a) The XANES for bulk $La_{1-x}Sr_xCoO_3$ samples (x=0, 0.15, 0.2, and 0.3); (b) the XANES for nanoparticle $La_{1-x}Sr_xCoO_3$ samples (x=0.15, 0.20, 0.25, 0.30, and 0.35). The insets show an expanded view of the pre-edge features. All data were collected at T=4 K.

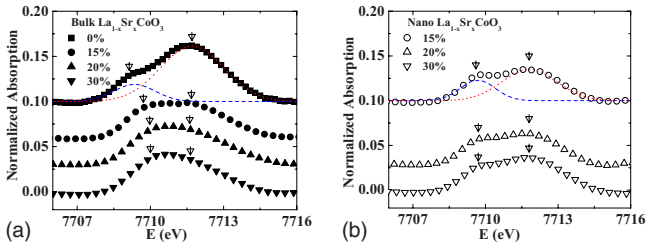

FIG. 2. (Color online) (a) The pre-edge structure after background-removal for bulk $La_{1-x}Sr_xCoO_3$ samples (x=0, 0.15, 0.2, and 0.3); (b) Similar pre-edge structure after removing the background for nanoparticle $La_{1-x}Sr_xCoO_3$ samples (x=0.15, 0.25, and 0.35). The open arrows show the positions of the two Gaussian peaks obtained from the fit to the pre-edge structure. Examples of the fits are shown, for bulk x=0 and nano x=0.15, as dashed and dotted lines obtained from the fit to the pre-edge structure. All data were collected at T=4 K. Data have been shifted vertically for better comparison.

that the shift with increasing temperature from 4–300K, is less than 0.15 eV for all samples.

The lack of a shift is in marked contrast to the similar system $La_{1-x}Ca_xMnO_3$ for which the Mn K-edge shifts about 3 eV for a valence change from Mn^{+3} to Mn^{+4}.[38] The shift in the Co K edge in $LaMn_{1-z}Co_zO_3$ is also about 3 eV as Co changes from Co^{+2} to Co^{+3},[39] and similar Co K-edge shifts are observed in other compounds for a valence change from +2 to +3.[40] For cobalt systems with a higher formal Co valence such as Na_yCoO_2, a similar edge shift of ~3 eV/valence unit is also observed as y decreases from 1 to about 0.5 (valence of Co changes from 3 to 3.5).[41] However, for yet smaller values of y, the Co edge no longer shifts upward.

We also investigated briefly the small Co K-edge pre-edge structure (between 7708 and 7714 eV), which shows two small peaks (better resolved for the nanoparticle sample). At the scale shown in the insets of Figs. 1(a) and 1(b), for both bulk and nanoparticle Sr-doped samples, the pre-edge structure shows little change with increasing Sr concentration above x=0.15. The largest change is between the doped and undoped samples; for x=0.0, the higher peak (~7712 eV) is significantly stronger, while the lower peak is slightly weaker at 4 K, compared to the Sr-doped samples. For $LaCoO_3$ at 300K, the lower peak increases slightly while the upper peak decreases 25–30%, and the pre-edge is then more similar to the doped samples. Toulemonde *et al.* reported a similar temperature change for $LaCoO_3$ between 20 and 300K, but with a larger decrease in the higher peak.[42]

To better see the changes in the pre-edge peaks, we have subtracted the background (from the main edge—modeled by an arctan function) and fit the double-peak pre-edge structure to a sum of two Gaussians, centered at approximately 7709 and 7712 eV; a third broad peak around 7718 eV was included to improve the background removal. The expanded background-subtracted pre-edge structure is shown in Fig. 2.

In Fig. 2(a), we show the background-subtracted pre-edge structure for the bulk samples. Although the absolute change is small, we find a systematic variation of the pre-edge structure with Sr concentration. For $LaCoO_3$, the pre-edge structure is fairly well resolved as two Gaussian peaks; a smaller peak (peak amplitude ~0.02) at ≈7709.1 eV and a larger peak (about five times larger integrated intensity) at ≈7711.7 eV. The separation of these two peaks is 2.6 eV (x=0). As the Sr concentration increases, the lower peak shifts upward with a small decrease in intensity. For the higher energy peak, there is no significant energy shift but a large amplitude decrease from x=0 to x=0.15; above x=0.15, however, the intensity of the second peak changes very little. The positions of the two peaks from the two Gaussian fits are indicated by the open arrows on each plot. To better resolve the peaks and obtain good estimates of the relative intensities, particularly for the higher concentrations, will require higher resolution data.

For the nanoparticle samples, the pre-edge peaks are well separated [See Fig. 2(b)]. Compared to the bulk samples, the first pre-edge peak (at a similar Sr concentration) is slightly larger while the second peak is slightly lower, but these changes (≤20%) are within our errors. Also, the positions and intensities do not change significantly with the Sr doping, from 0.15 to 0.35. There may be a small amplitude change, but the uncertainty in the background subtraction introduces large amplitude errors. It should also be noted that, for both bulk and nanosamples, the lower energy pre-edge peak has a weaker T-dependence than the peak at higher energy.

B. XANES—discussion

For increasing x, the lack of a significant shift in the main edge position, above that for $LaCoO_3$ (Co^{+3}) is surprising, as in the literature many assume a mixture of Co^{+3} and Co^{+4} with divalent doping on the La site.[3,7,42–46] However, this is predicated on the valence of O being −2 (i.e., an essentially filled $2p^6$ configuration). At x=0.35, the formal Co valence would then be 3.35 and one would therefore expect a ~1 eV edge shift based on edge shifts for other Co oxides as discussed above. The lack of a shift suggests that the doping achieved by adding Sr does not significantly remove electrons from the Co atoms in either the bulk or nanoparticle samples. The shift of an edge in an oxide system is determined by (1) the average bond length[47,48] and (2) transferred charge on the atom of interest. Usually, these two effects cannot easily be separated because an increasing valence is usually accompanied by a decreasing bond length and some charge transfer.

Several limited XANES studies have also been reported in the literature for $La_{1-x}Sr_xCoO_3$; some have investigated undoped material ($x=0$) (Refs. 49–51) while others present the dependence with Sr concentration at 100 K,[45] or at 300K.[52] None report a full temperature dependence for the Sr-doped samples from 4 to 300K. Two papers[49,52] appeared to use a different energy calibration and in those reports, the edge positions are shifted to lower absolute energies relative to other papers and the present results. Consequently, for those papers[49,52] we only considered relative shifts.

For all samples, the small Co *K*-edge shifts we have observed with Sr concentration, in both bulk and nanoparticle samples, are similar to other reports. Hanashima *et al.* measured the Co *K*-edge XANES for LSCO samples,[52] for $0 \leq x \leq 0.6$, and report a 0.7 eV shift in the white line peak over this large Sr concentration range. The shift in the main Co *K* edge is smaller than for the white line, especially for $0 \leq x \leq 0.3$. The actual shift in the main edge is difficult to estimate in their figures,[52] but is about the size of the symbols and clearly ≤ 0.2 eV. Sikolenko *et al.* also report a lack of a significant *K*-edge shift for a few samples.[45]

More importantly, however, none of these studies commented on the apparent lack of a change in the Co($3d$) configuration with increasing Sr concentration. The only work that addresses the Co($3d$) character is Ref. 53, but they only considered high Sr concentration samples for x above 0.5. For these high concentrations, they also saw no edge shift and noted that for this range, the holes introduced via Sr doping had little Co $3d$ character.

The lack of an edge shift for the Co edge, and hence a lack of change in the effective Co valence (as opposed to the formal Co valence, $3+x$) with increasing x is important, as the electron configuration about Co is crucial for understanding the magnetism. A related means of estimating the effective Co valence is to use the bond-valence sum approach which uses a sum over the nearest-neighbor distances.[54,55] For the $La_{1-x}Sr_xCoO_3$ system, diffraction studies by Caciuffo *et al.*[56] show that the Co-O bond length changes very little with Sr concentration (For $LaCoO_3$, $r_{Co\text{-}O}=1.924$ Å, and for $0.10 \leq x \leq 0.3$, the bond length is 1.927 ± 0.0005 Å); there is also very little change with T (<0.001 Å) up to 300 K.[56] Other diffraction studies also show very little change in the Co-O bond length (≤ 0.01 Å) for $0 \leq x \leq 0.4$, although the concentration dependence of the change is slightly different.[57,58] The Co-O bond length in our EXAFS analysis in Sec. III D 1 is also constant to 0.01 Å. Thus, the lack of an edge shift is, in fact, consistent with the nearly constant Co-O bond length in the Sr-doped samples.

The bond-valence sum approach relates the effective valence of an ion to a sum of either power law or exponential functions, over the nearest-neighbor bond lengths; here, we use the exponential form. Since the six Co-O bond lengths are all the same in $La_{1-x}Sr_xMnO_3$ the Co valence is given by[54,55]

$$V = 6e^{(r_o - r_{Co\text{-}O})/B} \tag{3}$$

and

$$\frac{dV}{V} = -\frac{dr_{Co\text{–}O}}{B}, \tag{4}$$

where r_o and B are constants.[54,55] This shows explicitly that an increased valence corresponds to a shorter bond length; then using $B=0.37$,[55] to increase the valence by 0.3 (for $x=0.3$) would require a significant bond-length contraction of ~ 0.037 Å, which is not observed. The valence calculated from the above equation, using the Co-O bond length, is about 3.1; it varies slightly for slightly different sets of constants, r_o and B.[54,55] Thus, both the bond-valence sums and the main Co *K*-edge position indicate that the electron configuration about Co remains very close to that of Co^{3+} as the Sr concentration increases.

Several authors[45,49–52] have also considered the pre-edge structure, and have usually assumed that it is a mixture of allowed quadrupole transitions and (forbidden) dipole transitions made partially allowed via hybridization of the central-atom Co($3d$) states, with p states [O($2p$) and Co($4p$)] and with neighboring Co($3d$) states. Further, most suggest that the first peak is a transition to the (nearly full) Co t_{2g} and the second peak a transition to the (essentially empty) e_g states.

However, a recent resonant x-ray emission spectroscopy investigation by Vanko *et al.*[59] convincingly shows that the first pre-edge peak in $LaCoO_3$ (at ≈ 7709 eV) is a nearly pure $1s$-$3d$ quadrupole transition; in this study, they used a single-crystal sample and found a strong intensity variation of this peak when the x-ray polarization was rotated relative to the crystal axes. In contrast, the larger peak at ≈ 7712 eV shows no angular variation and is therefore a weak dipole transition made allowed via hybridization. A similar hybridization model for making $1s$-$3d$ dipole transitions partially allowed was used earlier for the manganites.[38,60] Vanko *et al.* argue that both peaks are transitions to e_g final states and attributed the separation between these two peaks, (≈ 2.5 eV for $LaCoO_3$ in their data) as due to differences in the "core-hole screening" for the different transitions—the core-hole effect will be strongest for the quadrupole transition where the final state is on the central atom, and shifts the quadrupole transition to lower energy. This proposed assignment is consistent with our results; note that the first pre-edge peak shifts upward with increasing Sr concentration. $LaCoO_3$ is an insulator, but $La_{1-x}Sr_xCoO_3$ becomes conducting at higher Sr concentrations. Consequently, the bandwidths of states near the Fermi energy should increase for higher Sr concentrations, and the interaction with the core-hole potential will be smaller. In that case, the quadrupole transition should have a smaller shift to lower energies (i.e., moves to higher energies) as we observe.

If that proposal is correct it suggests that for the nanoparticle samples, the lack of a shift in the first (quadrupole) peak implies that the hybridized bands broaden less and likely that the nanoarticles are not conducting.

To summarize, we find very little shift (<0.15 eV) of the Co *K* edge with Sr concentrations up to $x=0.35$ for nine bulk and nanoparticle samples, and a similar tiny shift with T from 4–300K. These results indicate that the holes added via Sr doping are not localized on the Co atoms. Consequently, these holes must go elsewhere and must be localized more

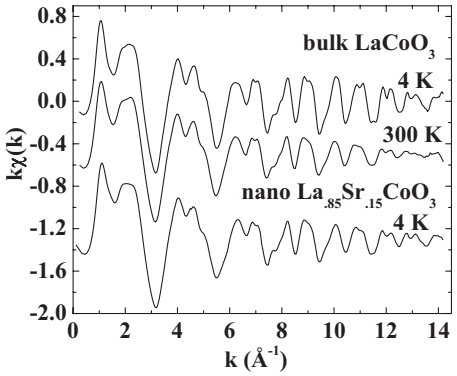

FIG. 3. Examples of k-space data for the pure compound $LaCoO_3$ measured at 4 (top) and 300 K (middle), as well as the k-space data for 15% nanoparticle LSCO at 4 K (bottom). The signal amplitude decreases at high T, but the signal to noise ratio of the data is good up to $k=13.3$ Å^{-1} at 300 K. Also note that, at 4 K, the data for the nanoparticle sample have a smaller amplitude than for the bulk sample above $k\approx 5$ Å^{-1}.

on the O($2p$) sites; these states are hybridized with the Co($4p$) and the Co($3d$) states. Such holes in the O bands will be the charge carriers—and the coupling of the unpaired O spins to the Co system may also be important for magnetism.

There is in fact evidence for increased holes in the O bands from O K-edge XANES studies; the beginning of the O K-edge shifts to lower energy with increasing Sr concentration and there is increased absorption at the main edge near 543 eV.[10,42] Note that if O were purely ionic with a −2 charge and therefore a $2p^6$ configuration, the $1s$-$2p$ transition would not be possible; however, there is considerably covalency in the transition-metal oxides and $1s$ to $2p$ transitions are observed in all of them at the O K edge. The observed increase in the O K-edge amplitude suggests that additional holes are present in the O bands—which are hybridized[42] with the Co($3d$) states.

C. EXAFS data

Examples of the k-space EXAFS data $[k\chi(k)]$, extracted as described previously, are shown in Fig. 3 for the pure bulk compound $LaCoO_3$ at 4 and 300 K, and for a nanoparticle sample (15%). At low T, the signal to noise is very good out to 14 Å^{-1} and comparable for all samples; however, it deteriorates at high k as the temperature increases and is poor beyond about 13.3 Å^{-1} at 300K. Consequently in all the fits the upper end of the FT k range is restricted to 13.0 Å^{-1}.

Next, the k-space data $k\chi(k)$ were fast Fourier transformed (FFT) to r space with a k-space window of 3.3–13.0 Å^{-1} and a Gaussian broadening of width 0.2 Å^{-1}; examples for the bulk samples are shown in Fig. 4. The first peak around 2 Å is the Co-O, and the second peak around 3 Å is a combination of Co-La/Sr, Co-Co, and some multiscattering peaks. Note that the position of the EXAFS peak does not reflect the real distances of the neighboring atoms about Co, since there is a phase shift $[2\delta_c(k)+\delta_i(k)$ in Eq. (1)], which shifts the peak position in the EXAFS plot to shorter r. For each sample, the amplitude is highest at low

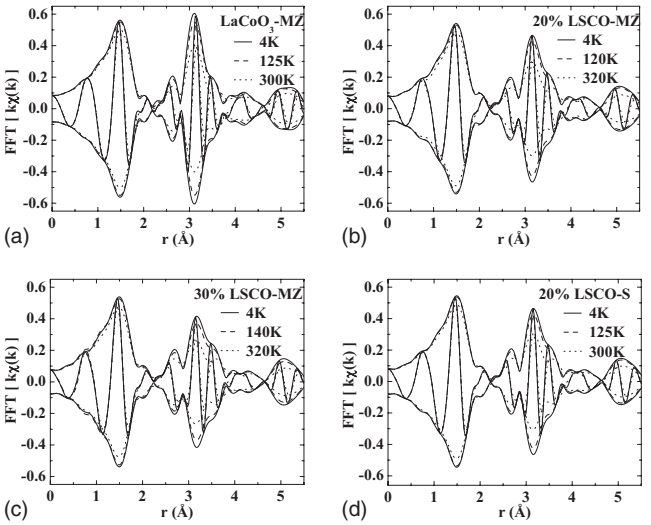

FIG. 4. Examples of r-space data [Fourier Transform of $k\chi(k)$] for bulk samples: (a) $LaCoO_3$ made by Mitchell and Zheng (MZ) (4, 125, and 300 K) with a k-space window of 3.3–13.0 Å^{-1} and a Gaussian broadening of width 0.2 Å^{-1}; (b) Similar r-space data for the 20% LSCO sample made by MZ (T=4, 120, and 320 K); (c) Corresponding r-space data for the 30% LSCO sample made by MZ (T=4, 140, and 320 K). (d) Data for the 20% LSCO sample made by Sundaram (S) (T=4, 125, and 300 K). Note that the plots in (b) and (d) are nearly identical. For all data, the amplitude is highest at low temperature (4 K) and decreases monotonically with increasing temperature. In this and all other r-space plots the fast oscillation is the real part (Re) of the FT while the envelope functions are $\pm\sqrt{\mathrm{Re}^2+\mathrm{Im}^2}$; Im is the imaginary part of the FT.

temperature and decreases monotonically with increasing temperature. Also we point out that the data for the two bulk samples (20%) made by different sample makers [Figs. 4(b) and 4(d)] are essentially identical, indicating that the structure and disorder are the same in the two samples. The first peak (Co-O) is nearly identical for all concentrations as reported earlier[35] while the second multipeak (2.8–3.8 Å) is smaller for the doped samples as a result of varying contributions for Co-La and Co-Sr. Note that the temperature dependences are also very similar. Thus, there are no large structural changes that can be associated with the significant changes in the magnetic properties with increasing Sr content.

Similar r-space data for the nanoparticle samples are shown in Fig. 5. The amplitudes of the first peak (Co-O) are nearly identical to those in Fig. 4 for the bulk and have similar temperature dependencies. Thus, any disorder/distortion of the O octahedra about each Co must be comparable in both nanoparticle and bulk samples. A much larger effect occurs, however, for the further neighbors—the amplitudes for the nanoparticle samples are considerably reduced compared to the bulk. Because the size of the nanoparticles ranges from 10 to 50 nm, with some particles possibly being multigrained, one might attribute this faster decrease in part to a size effect. We address this issue after fitting the data for the further neighbor peaks.

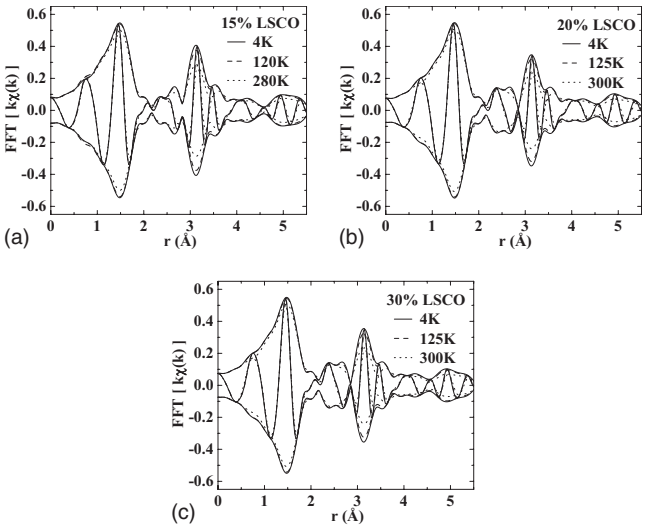

FIG. 5. Examples of *r*-space data for nanoparticle samples: (a) 15% $La_{1-x}Sr_xCoO_3$ sample measured at $T=4$, 120, and 280 K; (b) 20% Sr sample measured at $T=4$, 125, and 300 K; c) 30% Sr sample measured at $T=4$, 125, and 300 K. All the nanoparticle samples are made by SA, and the FFT *k*-space window is 3.3–13.0 $Å^{-1}$ with a Gaussian broadening of width 0.2 $Å^{-1}$. Note that the amplitudes of the further neighbor peaks ($r>2.5$ Å) are significantly smaller than for the bulk. A comparison of the first peak (Co-O) for the nanoparticle and bulk samples shows that this peak is comparable in both types of samples.

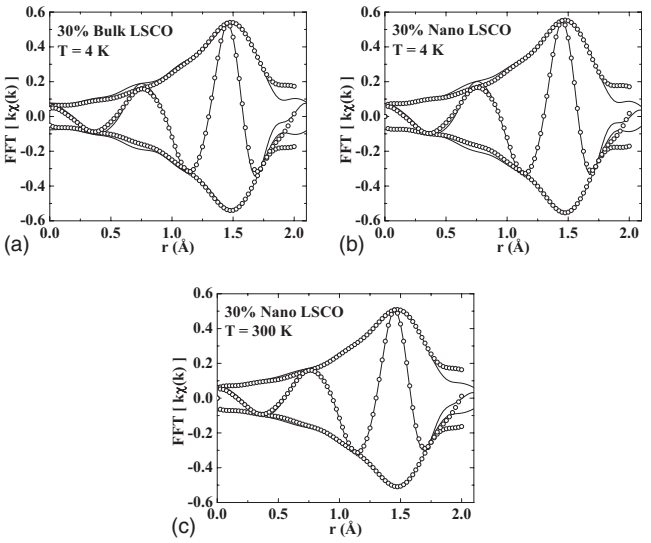

FIG. 6. Examples of the data and the fit for (a) the 30% Sr-doped bulk sample at 4 K; (b) 30% Sr-doped nanoparticle sample at 4 K and (c) the 30% nanoparticle sample at 300 K; data-solid line, fit-open circle. The *k* range for all fits is from 3.3 to 13 $Å^{-1}$, the fit range is from 1.1 to 1.6 Å. The fit quality does not change much when the temperature increases from 4 to 320 K.

D. Fits and results

In most of the literature, the $La_{1-x}Sr_xCoO_3$ system has the rhombohedral structure at low Sr concentration and low temperature. With increasing temperature or Sr concentration, the lattice structure eventually transitions to the cubic structure; for example, for $La_{0.6}Sr_{0.4}CoO_3$, the transition temperature is between 500 and 600 K.[44] Since all the Sr concentrations for our samples are below 35% and $T\leq 320$ K, we will use the rhombohedral structure ($R\bar{3}c$) (Ref. 61) to calculate the theoretical EXAFS functions (from FEFF),[62] which are used to fit our EXAFS data. Under this symmetry group, the six nearest Co-O bonds (~1.934 Å) have the same length; similarly, the Co-Co pair distance is ~3.825 Å. In contrast, the eight Co-La/Sr pair-distances will split into six longer distances (~3.326 Å) and two shorter ones (~3.273 Å).

1. Shortest Co-O

In this section, we describe fits of the first Co-O peak (fit range is from 1.1 to 1.6 Å) using a single peak fit; in the next section, we use these results to extend the fit of the data to the rhombohedral structure described above, over a longer range (1.2 to 4.1 Å).

The first peak was fit to a theoretical Co-O EXAFS function generated by FEFF 8.20 (developed by Rehr and co-workers),[62] using the program RSFIT (RSXAP package). The FEFF calculations were based on the rhombohedral structure,[61] which has one Co-O bond-length ~1.934 Å. Our primary interest here is the width of the Co-O pair distribution function, which parametrizes the amount of distortion present around Co. We fixed the number of oxygen neighbors to the coordination number ($N_1=6$ neighbors) for each sample. To minimize the number of free parameters, a number of other parameter constraints are also required. First, for data collected on the same sample at the same experiment, ΔE_0 was obtained by allowing σ, r, and ΔE_0 to vary for the low-temperature data (two temperatures, three scan each); the average value of ΔE_0 obtained from those fits was used to constrain ΔE_0 for the rest of the data in the same set. Uncertainties in ΔE_0 limit the absolute error for r to about 0.01 Å; relative errors can be much better. We determined the parameter S_0^2 in a similar way. for fits of the low-temperature data which have the best signal-to-noise ratio, we let the amplitude $A_1(A_1=N_1S_0^2)$ vary and determined an average value of S_0^2 from those fits. Then, A_1 was kept constant in all the fits at higher temperatures. For all the LSCO data, the averaged $S_0^2\approx 0.8$, so the A_1 we used is 4.8 for all samples. Small errors in S_0^2 lead to a static vertical shift in the entire data set in plots of σ^2 vs T. Note that an error in S_0^2 primarily shifts the origin slightly but has little effect on the T-dependence of σ^2.

In Fig. 6(a), we show the fit for the 30% Sr-doped bulk sample data at 4 K, and in Figs. 6(b) and 6(c) show similar fits for a 30% nanoparticle sample at 4 and 300 K. The goodness of fit is comparable for all fits including the fits at 4 and 300 K. From these fits, we extracted the Co-O bond distance r and the width σ of the PDF. The values of r agree very well with diffraction within 0.01 Å; in particular for $LaCoO_3$, we see almost the same temperature dependence for $r_{\text{Co-O}}$ as observed in diffraction for the lattice parameter[63]—$r_{\text{Co-O}}$ (as well as $r_{\text{Co-Co}}$) is constant to about 40 K and then increases nearly linearly up to 300 K. Because of the good agreement for r, between our results and diffraction, the values of r will not be discussed further. For each sample, we obtained a plot of σ^2 vs T.

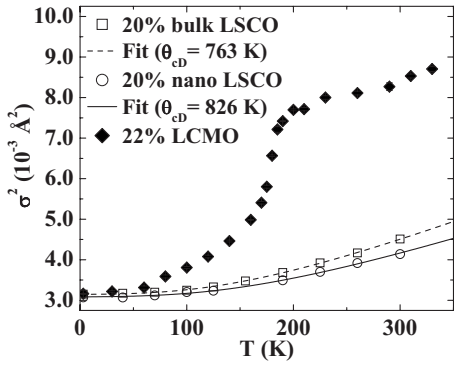

FIG. 7. Comparison of $\sigma^2(T)$ for different systems: the 20% LSCO bulk sample (open square) and its correlated Debye fit (dash line), the 20% LSCO nanoparticle sample (open circle) and its correlated Debye fit (solid line), and the corresponding results for a 22% Ca-doped $La_{1-x}Ca_xMnO_3$ sample (LCMO)-solid diamonds; the LCMO sample has a large JT distortion that develops between 100 and 190 K.

The thermal phonon contribution to $\sigma^2(T)$ was determined from a fit of $\sigma^2(T)$ (4-320 K) to the correlated Debye model [Eq. (5)] plus a static offset. This model is usually a good approximation for all phonon modes,[64] including acoustic and optical phonons, and is given by[65–67]

$$\sigma^2_{c\mathrm{Debye}} = \frac{3\hbar}{2M_R}\int_0^{\omega_D} \frac{\omega}{\omega_D^3} C_{ij}\, coth\left(\frac{\hbar\omega}{2k_BT}\right) d\omega, \qquad (5)$$

where ω_D is the Debye frequency, C_{ij} is a correlation function given by $1\text{-}\sin(\omega r_{ij}/c)/(\omega r_{ij}/c)$, $c=\frac{\omega_D}{k_D}$ where k_D is the Debye wavenumber, and $\sigma^2_{c\mathrm{Debye}}(T\sim 0)$ with $\sigma^2_{\mathrm{static}}=0$, gives the zero-point motion value of σ^2. The slope of $\sigma^2_{c\mathrm{Debye}}(T)$ vs T is very low at low T and increases to a constant value (determined by the spring constant, reduced mass, and C_{ij}) for $T>\Theta_D$. See Ref. 66 for details.

In Fig. 7, we compare the $\sigma^2(T)$ results for the Co-O bond in a 20% LSCO bulk sample with the 20% LSCO nanoparticle sample; the correlated Debye fits (dashed and solid lines) are also plotted. We also plot for comparison, corresponding results for a 22% Ca-doped $La_{1-x}Ca_xMnO_3$ sample[32] which has a metal-insulator (MI) transition around 190 K that is coupled with a Jahn-Teller distortion of the Mn-O PDF. At low T, there are six nearly equal Mn-O bond lengths; a JT splitting develops between 100 and 190 K, and results in a configuration with two longer Mn-O bonds, ~2.1 Å, and four relatively shorter bonds with an average bond length of 1.95 Å.[68] The proposed JT distortion of the Co-O PDF[34] is of comparable magnitude to that observed in LCMO; however, we recently found no evidence for a distortion of this magnitude for bulk samples.[35] The $\sigma^2(T)$ results for the Co-O peak of the nanoparticle particle samples are nearly identical to those for the bulk samples; thus, we find no evidence for any step in $\sigma^2(T)$ that would indicated the formation of a significant JT distortion of the Co-O bonds in any of the cobaltite samples.

σ^2 vs T plots were reported earlier for all the bulk samples except the 15% sample.[35] These plots followed a simple correlated Debye model well. The static distortions at low T are also small and range from $0.3–7.8\times10^{-4}$ Å, comparable to our uncertainty in σ^2. Thus, this small static value is also inconsistent with a significant JT splitting at low T. The average correlated Debye temperatures (θ_{cD}) for all bulk samples is approximately 775 K with an estimated uncertainty (including systematic errors) of ~30 K. Details for bulk samples are provided in Table II for comparison with the nanoparticle samples discussed below. The 15% Sr sample has a slightly higher value for θ_{cD}, 813 K and a comparable value of $\sigma^2_{\mathrm{static}}$, when compared to the other bulk samples.

TABLE II. Correlated Debye temperatures θ_{cD} and static distortions for all the bulk (top) and nanoparticle (bottom) samples. For the bulk samples the sample maker is indicated (MZ or S) in first column; all the nanoparticle samples were prepared by Sundaram and Anderson. Experiment No. 1 means the data were taken on the first experiment, etc., and the * indicates a data set with a short range in T. The errors shown for θ_{cD} are only from the scatter of the $\sigma^2(T)$ data; including systematic effects and the limited T range, the uncertainty is ~30 K.

Concentration	Exp. No.	θ_{cD}	$\sigma^2_{\mathrm{static}}$ (10^{-4} Å^2)
0.00(MZ)	2	762 ± 27	0.3
0.15 (S)	2	813 ± 7	6.7
0.20(MZ)	1	782 ± 17	6.7
0.20 (S)	2	763 ± 4	4.9
0.30(MZ)	2	756 ± 28	7.8
0.15	1	817 ± 29	5.6
0.15	2*	834 ± 12	11.2
0.20	2	826 ± 10	6.3
0.25	1	829 ± 17	7.8
0.25	2*	826 ± 11	12.7
0.30	2	832 ± 12	6.3
0.35	1	825 ± 12	6.0
0.35	2	818 ± 14	9.5

The results for the five nanoparticle samples (SA) are shown in Fig. 8. They are similar to the earlier bulk sample results with two differences. First, the results for the 15%, 25%, and 35% Sr-doped samples [Figs. 8(a), 8(c), and 8(d), respectively], show a systematic upwards shift in the $\sigma^2(T)$ plots for the second run (open symbols) compared to the first run (solid symbols). Yet other samples [$x=0.2$ and 0.3—see Fig. 8(b)], measured only in the second run, show the same value of σ^2 at low T as the other three samples did in the first run. The reason for such a systematic shift in σ^2 for only these three samples is unclear; however, since we found no significant change in the σ^2 data between the two experimental runs for the bulk samples (see Fig. 2(b) in reference)[35] it is very unlikely that the beam line was different for only the nanoparticle samples. (Note that data were collected for many samples at a given temperature and then the temperature was changed).

More likely, it is an aging effect—the old samples, both bulk powders and the nanoparticles, were mounted on tape

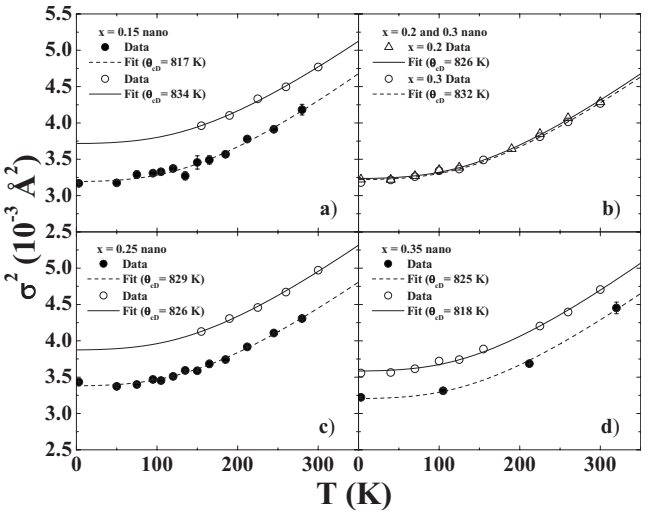

FIG. 8. σ^2 for the Co-O peak as a function of T for various nanoparticle samples ($0.15 \leq x \leq 0.35$), on the same vertical scale. The solid circles and triangles represent the data from the first measurement, open circles represent the data from the second measurement; the dash line is the fit for the first experiment, while the solid line is the correlated Debye fit for the second experiment. (a) 15% Sr-doped LSCO; (b) 20% and 30% Sr-doped LSCO; (c) 25% Sr-doped LSCO; (d) 35% Sr-doped LSCO. For panels (a), (c), and (d), the second measurements (open circles) are on nanoparticles that were stored on tape for about one year.

and stored in a desicator—however, they remained in contact with the glue of the tape during the time the samples were stored. Other LSCO materials for which EXAFS samples had not yet been prepared, were stored as dry powders in sealed containers. Only the three nanoparticle samples that had been prepared for the first run and stored on tape showed this effect—bulk powders, also stored on tape, did not. This suggests a surface effect—possibly some oxidation at the surface. Such oxidation probably also takes place for the bulk samples, but the surface to volume ratio of the bulk powder is so small that it is negligible. Note that the tape-mounted nanoparticles were also exposed to high intensity x-rays, and this might contribute to the observed small increase in the disorder about Co in the aged nanoparticle samples stored on tape.

The second possible difference is that the average value of θ_{cD} for all the nanoparticles is slightly higher—825 K, compared to 775 K (See Table II for the individual values). However, because T is well below θ_{cD} the results are quite sensitive to the values of σ^2 near 300 K and systematic errors dominate—also the error bars overlap slightly. This 50 K difference in θ_{cD} is suggestive that the average Co-O bond might be slightly stiffer in the nanoparticles compared to the bulk particles. However, to verify that it is a particle size effect would require measurements on nanoparticles of various sizes, with a narrow particle-size distribution for each sample. Also, since the values of σ^2(4 K) are comparable for both the bulk samples and (nondegraded) nanoparticle samples, static distortions must be comparable.

Finally, we note that, for all the bulk and "non-aged" nanoparticle samples, σ^2(4 K) is close to the value for zero-point motion; the excess distortion is close to zero for bulk $LaCoO_3$, and varies from $5-12\times10^{-4}$ Å^2 for all the other samples. Thus, any JT distortion at low T must be very small.

2. Further neighbors

Before describing the fits of the further neighbor peaks in the EXAFS data, it is instructive to review the results from x-ray and neutron-diffraction studies. Most diffraction studies fit the data to a rhombohedral structure; LSCO is a very ordered structure with quite small changes in the lattice parameters and pair distances up to 300 K. However, the Co-O-Co bond angle does have a slight temperature and Sr concentration dependence. For example, as the temperature increases from 5 to 350 K, the Co-O-Co angle increases from about 163° to almost 164° in $LaCoO_3$.[63] The concentration dependent change is larger; at $T=2$ K, the Co-O-Co angle is 163° for the pure compound, and 167° for 30% LSCO (Ref. 56); a similar Sr concentration dependent change was also observed at room temperature.[57]

The small changes in lattice parameters and pair distances with T or x mean that variations in the pair distance of the calculated FEFF standards for the first few atom pairs are also small. However, a small change in the Co-O-Co angle has a large impact on the amplitude of the multiple-scattering (MS) peaks Co-O-Co and Co-O-Co-O when the Co-O-Co angle is close to 180°.[66] Then forward scattering through the O atom significantly enhances the multiple-scattering peak amplitude over that for the direct Co-Co single-scattering (SS) peak. We return to this aspect shortly.

To calculate the FEFF functions[62] for fitting our EXAFS data over the range 1.2 to 4.1 Å, we used the same rhombohedral $R\bar{3}c$ structure[61] as used for our nearest-neighbor (Co-O) fits. These FEFF functions include several SS contributions to the PDF: the shortest Co-O bond (~1.934 Å), an average Co-La/Sr distance (~3.313 Å), the Co-Co distance (~3.825 Å), and two longer Co-O pair distances at 4.1036 and 4.4618 Å, which have small tails within the r-space fit range. Because the Co-La/Sr distances have a small splitting (two neighbors at 3.273 Å, and six at 3.326 Å), we summed two Co-La functions with these distances and relative amplitudes and assumed they both have the same value of σ (and similarly for Sr). In addition, we also included four MS peaks up to ≈5 Å. For the initial fits, the FEFF function for the Co-O-Co MS peak was calculated for $LaCoO_3$ with a Co-O-Co angle of 163.2°.

Again, to reduce the number of free parameters, one must introduce constraints. We constrained the amplitudes of the single-scattering FEFF functions to the lattice structure, $A_i = N_i S_0^2$, where N_i is the coordination number for each atom-pair peak and S_0^2 is the amplitude reduction factor ($S_0^2=0.8$), obtained previously[35] from fits of the nearest-neighbor Co-O bond—see Sec.III D 1). We also weighted the Co-La and Co-Sr functions based on eight neighbors at the La/Sr site and the known Sr concentration; i.e., for $La_{1-x}Sr_xCoO_3$, the total amplitude of the Co-Sr peak is $6.4x$, while that for the Co-La peak is $6.4(1-x)$. We constrained all the SS distances to the lattice structure and only allowed one distance parameter to vary, corresponding to an overall expansion or contraction of the lattice. The broadening parameters (σ) for

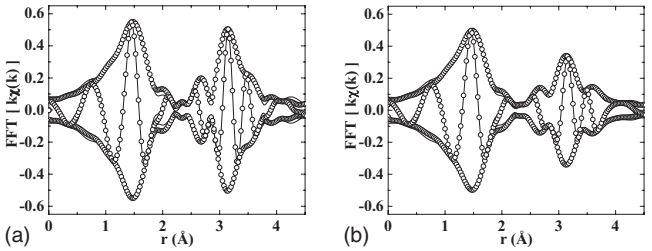

FIG. 9. (a) 4 K: 15% bulk data and the fit; (b) 300 K: 15% bulk data and the fit. In all figures, data are represented by solid lines, and the fits are open circles. Fit range 1.2–4.1 Å.

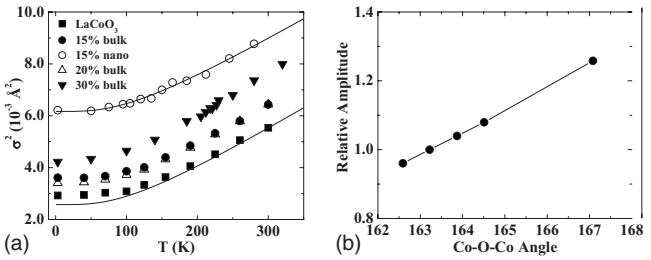

FIG. 10. (a) A plot of $\sigma^2(T)$ for the Co-Co bond, for all the bulk samples and the 15% nanoparticle sample as described in the text (using different Co-O-Co MS functions for each Sr concentration). The solid squares are for bulk $LaCoO_3$ (Co-O-Co angle ~163°), solid circles for 15% bulk LSCO and open circles for 15% nanoparticle LSCO (Co-O-Co angle ~164.6°), open triangles for 20% bulk LSCO (Co-O-Co angle ~165.2°) and solid triangles for 30% bulk LSCO (Co-O-Co angle ~167°). We also plot, using a solid line, the correlated Debye fit with a Debye temperature θ_{cD} =480 K and no static distortion ($\sigma^2_{\text{static}}=0$); this curve lies close to most of the bulk sample data. For the 15% nanoparticle sample we also fit to the correlated Debye model but in this case there is a significant static offset if we assume 6 Co neighbors ($\theta_{cD}=490$ K, $\sigma^2_{\text{static}}=3.6\times10^{-3}$ Å^2); if we assume it has a similar static distortion as the 15% bulk sample, the number of Co neighbors has to be about 30% less, which is equivalent to having the averaged particle size ≈2 nm if the particle size is the only cause of the reduction in Co neighbors. The relative errors (and fluctuations from point to point) are comparable with the size of the symbols; they are obtained from the variation of σ in three scans at the same temperature. The systematic error (a fixed vertical shift in all data points in a data set) is of order 5×10^{-4} Å^2. (b) A simulation of the relative amplitude of the Co-O-Co multiple-scattering peak vs Co-O-Co angle with no additional broadening for σ. The amplitude of the MS peak at ~163.2°, which is our starting value, is used as the reference value.

each of these SS peaks was allowed to vary independently with two exceptions: (1) the Co-La and Co-Sr peaks overlap and to reduce the number of parameters we set the ratio of these two parameters proportional to the inverse of the reduced masses; i.e., $\sigma^2_{\text{Co-Sr}}=\sigma^2_{\text{Co-La}}\ M_{\text{Co-La}}/M_{\text{Co-Sr}}$; (2) similarly we set the widths of the PDFs for the two longer Co-O distances (4.1036 and 4.4618 Å) equal.

The constraints on the four MS peaks are more complex. For the shortest (~3.3 Å) triangular O-O-Co paths and longest (~4.5 Å) paths, we constrained the R shift to the lattice structure, and constrained the σ to be the same as for the corresponding SS peaks; for the two MS peaks around 3.8 Å, we constrained them differently. One MS peak originates from the 180° back and forth scattering on the O-Co-O bond chains, so we constrained this peak to the Co-O peak, with an R shift twice that for Co-O and $\sigma\ \sqrt{2}$ times larger than $\sigma_{\text{Co-O}}$. The last MS peak is from the Co-O-Co bond chains; this peak overlaps the SS Co-Co peak and fluctuations of its length are comparable to the Co-Co path. Consequently, we constrained it to the Co-Co SS peak; i.e., the R shift was constrained to the lattice structure, and σ was set equal to that for the Co-Co peak.

This model, with the above constraints, fit the data well; no significant distortions were found in the LSCO system, and all the peaks remain close to the positions suggested by the diffraction results. (If the constraints were not reasonable, the fit would not be good or some parameter would be unphysical, and the constraints would need to be re-evaluated.) In Figs. 9(a) and 9(b), we show the 15% LSCO r-space data measured at 4 and 300 K as well as the final fits described below. It can be seen that the fits are very good from 1.2 to 4.1 Å at both 4 and 300 K, except for the middle region (1.8 to 2.3 Å) with low amplitude which is produced by the interference of the tails of the peaks at higher (~3 Å) and lower (~1.5 Å) r.

In our first set of fits, we used the same Co-O-Co MS reference peak (calculated with FEFF for the $LaCoO_3$ structure) for all fits. We found that σ^2 for the Co-Co (and Co-O-Co) peak decreased as the Sr concentration increased and for 30% Sr, $\sigma^2(T)$ was below the data for $LaCoO_3$; also $\sigma^2(4K)$ was well below the value calculated for zero-point motion. This was unexpected and is not physical, as substitution should lead to some increase in static disorder.

Diffraction studies of these systems indicate there is a change in the Co-O-Co bond angle (~163° for $LaCoO_3$ and ~167° for 30% bulk LSCO),[56,63] and this change was not considered in the above fits. Since the amplitude of the Co-O-Co MS peak depends quite strongly on the Co-O-Co angle θ for angles close to 180°,[66] this will control the value of $\sigma^2_{\text{Co-Co}}$ obtained in the fit when $\sigma^2_{\text{MS,Co-O-Co}}=\sigma^2_{\text{Co-Co}}$. The amplitude of the MS peak is often larger than the SS peak for angles above 150° and the correlation between amplitude and σ is such that if the amplitude of the FEFF function increases, the value of σ^2 needed to fit the data also increases.

We next calculated the MS peak as a function of the Co-O-Co angle (See Fig. 10) and compared it to that for $LaCoO_3$. We found a strong dependence—a ~5% amplitude change for a 1° change; thus the increasing Co-O-Co angle with Sr concentration cannot be ignored. For the fits, we therefore calculated the MS peak using the Co-O-Co angles obtained in diffraction at each Sr concentration.[56]

The $\sigma^2(T)$ results for Co-Co are plotted in Fig. 10(a). Including the increased Co-O-Co bond angle as the Sr concentration increases, leads to an increase in $\sigma^2(4$ K) and hence an increase in the static disorder as shown in Fig. 10(a). This is now consistent with the expected increase in disorder when doping with an atom of a different size. The correlated Debye temperature (θ_{cD}) from fits of the data, is about 480 ± 20 K; systematic errors increase the error to about ±30 K. The curvature of the $\sigma^2(T)$ data (and hence the value of θ_{cD}) does not change significantly with the

change in the Co-O-Co angle; it is only a static offset effect. Thus for the bulk samples there is no significant unusual distortion of the lattice with increasing Sr concentration—only a change in the average Co-O-Co bond angle and a small increase in static disorder.

In the literature, a T-dependence of the Co-O-Co bond angle is also reported (about 1° as T increases from 5 to 350 K),[56,63] though it is small compared with the Sr concentration dependence. This will slightly increase the values of $\sigma^2(T)$ at high T and hence decrease θ_{cD}. However, θ_{cD} will only change $\approx$10–20 K($<$4%), which is less than our estimated error.

In Fig. 10(a), we also plot $\sigma^2_{\text{Co-Co}}(T)$ for the 15% nanoparticle sample, which has a comparable $\theta_{cD} \approx 490$ K as bulk samples, but a much larger static distortion under the assumption of 6 Co neighbors; similar results are obtained for the other nanoparticle samples. For these materials, the excess static distortion may partially arise from the small size of the particles. By conducting a series of fits using different values of $N_{\text{Co–Co}}$ for the Co-Co (and Co-O-Co) peak, we found that to reduce $\sigma^2(4\ \text{K})$ to a value comparable to that for the 15% bulk sample, we need a reduction of $N_{\text{Co-Co}}$ by approximately 30% (4.2 Co neighbors instead of 6), which is equivalent to having nanoparticles with an averaged size of about 2 nm. However, this number is much smaller than the size obtained in TEM measurements, 10–50 nm. There are several possible explanations for this discrepancy: first, the particles observed in TEM may be clusters of much smaller nanoparticles; second, part of the nanoparticles may be amorphous; and third, the surface of the nanoparticles may be strained, leading to a range of bond lengths or Co-O-Co bond angles and a gradual variation of the structural parameters from the center to the outer shell. To investigate the latter, one would need to make a series of nanoparticle samples with narrow distributions of particle sizes. However, it will be difficult to separate three effects that reduce the EXAFS peak amplitude—(1) a reduction in the effective coordination number in small particles, (2) a broadened distribution of Co-O and Co-Co distances and, (3) for the Co-Co peak, variations in the Co-O-Co angle throughout the nanoparticle.

For the nanoparticle samples, if we use the same MS reference (same Co-O-Co bond angle) for the Co-O-Co multiscattering peak, we find a similar trend to the bulk samples, that the values for σ^2_{static} decreases with increasing Sr concentration. This suggests that, in the nanoparticle samples, there is also a similar Co-O-Co bond angle increase with increasing Sr concentration. However, EXAFS is not sensitive enough to tell exactly how this angle changes.

E. EXAFS—discussion

The main result from the analysis of the EXAFS data is a lack of evidence for a JT distortion, for both bulk and nanosamples. If we assume for the bulk material that this excess distortion all comes from a small fraction of sites with a JT distortion, then we can estimate the maximum fraction of JT distorted sites required to produce this small excess contribution at low T [we take a conservative assumption that the JT splitting $\sim$0.15 Å, close to the value in the CMR manganites, although Louca and Sarrao reported a range of Co-O bond-length splittings from 0.17 Å (Ref. 14) to 0.24 Å (Ref. 69) in cobaltites]. For this simulation, we start with the measured value of σ^2 at low T and add the effect of a percentage of JT split sites; we assumed there are four short and two long Co-O bonds, split by 0.15 Å. The increase in σ^2 with an increasing fraction of JT split Co-O distribution is plotted in Fig. 11(a); the shift is the same whether we start with a small or large value of σ^2 (e.g., at low or high T). Using this plot and assuming that all the excess static distortion ($\sigma^2_{\text{static}} = 7 \times 10^{-4}$ Å^2) is from a JT splitting, an upper limit to the fraction of JT split sites in the sample is $\sim$15%. However, since some static disorder is expected from Sr doping, a reasonable upper limit must be considerably lower, $\leq$10%.

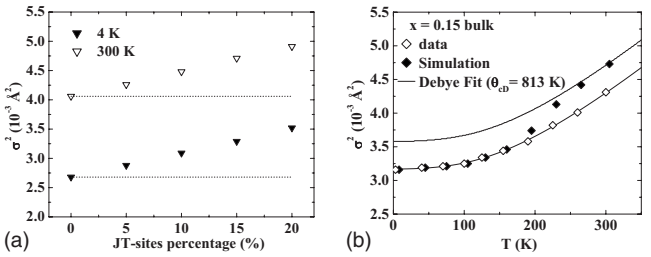

FIG. 11. (a) The calculated increase in σ^2 vs the percentage of Jahn-Teller distorted sites for pure bulk $LaCoO_3$ sample at 4 and 300 K, the solid triangles are the simulated results at 4 K, while open triangles are at 300 K, the dotted-line is a guide to the eye. (b) Simulation assuming that 10% of the Co sites have a JT distortion develop between 150 and 250 K for the 15% bulk $La_{1-x}Sr_xCoO_3$ sample. The JT contribution to σ^2 would produce a small step in σ^2; the lower solid line is the correlated Debye fit to the data below 150 K, while the upper one is a shift in the lower line to overlap with the simulation at higher temperature.

We can do similar simulations assuming a fraction of sites develop a JT distortion over some range of T, say 100 K. Our data shown in Fig. 8 [and Figs. 2a and 2b in Ref. 35] show no evidence of a step between 50 and 300 K. Our simulations [see Fig. 11(b) and also Fig. 2a in Ref. 35] suggest that a step, corresponding to 10% of the sites having a JT distortion, would be observed.

Our results agree out to the third neighbors with the $R\bar{3}c$ space group obtain in most diffraction studies. However, it should be noted that one high-resolution x-ray diffraction study suggests that the pure compound $LaCoO_3$ has the monoclinic ($I\bar{2}a$) symmetry.[70] The difference between the rhombohedral and monoclinic structure is that the latter space group has more distortion of the environment about Co, such that the shortest Co-O bonds split into three groups, two at 1.874 Å, two at 1.925 Å, and the other two at 1.993 Å.

We can test this model by comparing the value of σ^2 extracted in a single peak fit (for $R\bar{3}c$) of the $LaCoO_3$ data, with that for the split Co-O peak in space-group $I\bar{2}a$; for the latter fit, we impose the splitting of the Co-O bond lengths ($\sim$0.06 Å) reported in diffraction.[70] For the single peak fit of the data at 4 K, $\sigma^2 = 0.0026$ Å^2. For the three peak fit we use the same value of σ for each of the three peaks—the

result is that $\sigma^2 \leq 0.0001$ Å^2, an unphysically low result as at 4 K the minimum value of σ^2 should be given by zero-point motion. We can, in fact, calculate the effect of splitting a peak in the broadening of any PDF. For three peaks at r_o and $r_o \pm \delta r$; $\delta r = 0.06$ Å, the effective static contribution to σ^2 from the split peak, is $2/3 \times (\delta r)^2 \sim 0.0024$ Å^2. Thus, if a single peak fit has $\sigma^2 = 0.0026$ Å^2, the effect of modeling it as three peaks will be to lower σ^2 by 0.0024 Å^2, which is consistent with what we observe. Thus, our data are inconsistent with a splitting of the Co bond distances into three groups separated by 0.06 Å. However, if a much smaller monoclinic splitting were present, <0.03 Å for which σ^2_{static} would be <0.0006 Å^2, we could not rule it out.

IV. SUMMARY AND CONCLUSIONS

Our EXAFS/XANES measurements show two important results: first, the XANES data (Sec. I) show no significant Co *K*-edge shift as a function of either Sr concentration or temperature. This result is generally consistent with the limited data reported in the literature. Second, the EXAFS analysis finds no evidence for a Jahn-Teller distortion of the nearest-neighbor Co-O bond for any samples, of either bulk or nanoparticle material (Sec. III D 1) in contrast to earlier neutron PDF studies.[34] Any net distortion, if it exists, is very small, or corresponds to a small fraction of the Co sites. If we assume, for the bulk material, the excess distortion at low *T* all comes from a small fraction of sites with a JT distortion, then we can estimate the maximum fraction of JT distorted sites—from 10–15%; it would be less than 5% if the JT splitting were 0.24 Å. However, since some static disorder is always expected, our results are consistent with no JT distortions about Co.

In addition, the lattice structure changes very little with Sr concentration or temperature. The EXAFS analysis is consistent with diffraction results for the $R\bar{3}c$ space group[56,63] and with the results of recent neutron PDF experiments,[36] but not with the proposed $I\bar{2}a$ space group[70] with three Co-O peaks split by ~ 0.06 Å.

The lack of a Co *K*-edge shift indicates that the effective Co valence [the Co(3*d*) configuration] remains nearly constant as the Sr concentration increases for the $La_{1-x}Sr_xCoO_3$ system. The lack of an edge shift is, in fact, consistent with the nearly constant bond lengths and lattice parameter observed in diffraction studies,[56,63] and with the bond-valence sum model which relates changes in valence to average changes in bond length.[54,55] Although a similar lack of any significant shift has been reported previously,[45,52] the issue has not been discussed in detail. In particular, this result raises the question—where are the holes located that are introduced via Sr doping? We propose that such holes are found mainly on the O sites and that these O holes lead to the conductivity of the samples. Oxygen *K*-edge XANES clearly show an increased amplitude and shift to lower energy as the Sr concentration increases.[10,42] The unpaired spin on some O atoms may also couple with a few magnetic Co moments via Co(3*d*)-O(2*p*) hybridization, to produce the unusual magnetic properties observed in the cobaltites. Often, the $La_{1-x}Sr_xCoO_3$ system is discussed in terms of a mixture of ionic Co^{3+} and Co^{4+}, but in view of these new results, it appears that the 3*d* character of the Co atoms changes little with Sr doping, and models used to describe the cobaltites need to be modified and extended.

The lack of a JT-like distortion about the Co atoms for either bulk or nanoparticle samples is strong evidence against a localized intermediate spin (IS) state for Co. There is no evidence for a step increase in the broadening of the Co-O PDF such as is observed for the Mn-O PDF in the CMR manganites,[32,71] or any significant excess static distortion at low *T* that might indicate a JT distortion at low temperatures. The IS state requires a single electron in the Co e_g state and such a configuration is expected to be JT active, whereas LS and HS states are not. Our local structure measurements therefore support models in which the magnetization arises from a mixture of LS and HS configurations, (with possibly a coupling to a small fraction of unpaired O spins). The only ways in which a significant fraction of Co might have a single e_g electron configuration and yet not show a JT distortion, are if (1) the e_g electrons were hopping so fast that the lattice could not respond or (2) there is a large spin-orbit coupling.[21] However, if the added mobile holes are localized mostly on the O atoms, as suggested by the XANES and bond-valence calculations, then the hopping charges are not e_g electrons localized mainly on Co. Further, if holes in the O bands are the dominant charge carriers, it is not clear that spin-orbit coupling is important for the e_g states. These combined results therefore suggest that quasilocalized Co e_g states are not singly occupied. It may be that the extended nature of the electron states is a crucial feature for the cobaltites and one should not try to describe the system using localized concepts.

The results for the nanoparticles are very similar to those for the bulk materials with the main difference being a rapid decrease in the EXAFS peak amplitude with increasing *r*. This indicates either fewer neighbors as a result of reduced particle size or increased disorder in the nanoparticles; it is likely a combination of both. Another significant difference is in the double-peak structure of the pre-edge attributed to Co(3*d*) states; for the bulk material the lower peak position moves up in energy with increasing Sr concentration while for the nanoparticle samples, the position of these two peaks remain constant. Since the magnetization of the nanoparticles is an order of magnitude smaller than for the bulk material it may be related to this small difference of the pre-edge structure.

Theoretical results vary considerably depending on various assumptions and the assumed lattice structure ($R\bar{3}c$); many do not include a JT distortion. Several suggest only e_g states just above E_F, while others show some t_{2g} states as well. Further calculations are needed which include the possibility of holes in the O bands, with little change in the Co(3*d*) configuration, as well as the consequence of having a fraction of Co sites with a significant JT distortion.

ACKNOWLEDGMENTS

We would like to thank Gey-Hong Gweon, George Sawatzky, and John Freeland for helpful discussions regarding

our experimental results, and Jacob Stanley for help collecting data. Work at UCSC was partly funded by DOE under Grant No. DE-FG02-05ER46181. The work at Argonne (J.F.M. and H.Z.) was supported under Contract No. DE-AC02-06CH11357 by U. Chicago Argonne, LLC, Operator of Argonne National Laboratory, a U.S. Department of Energy Office of Science Laboratory. The EXAFS experiments were performed at SSRL (operated by the DOE, Division of Chemical Sciences, and by the NIH, Biomedical Resource Technology Program, Division of Research Resources).

[1] A. P. Ramirez, J. Phys.: Condens. Matter **9**, 8171 (1997).
[2] M. Itoh, I. Natori, S. Kubota, and K. Motoya, J. Phys. Soc. Jpn. **63**, 1486 (1994).
[3] D. Louca, T. Egami, and G. H. Kwei, J. Supercond. **12**, 291 (1999).
[4] M. A. Senaris-Rodriguez and J. B. Goodenough, J. Solid State Chem. **118**, 323 (1995).
[5] P. S. Anil Kumar, P. A. Joy, and S. K. Date, J. Phys.: Condens. Matter **10**, L487 (1998).
[6] V. V. Sikolenko, A. P. Sazonov, I. O. Troyanchuk, D. Tobbens, U. Zimmermann, E. V. Pomjakushina, and H. Szymczak, J. Phys.: Condens. Matter **16**, 7313 (2004).
[7] H. M. Aarbogh, J. Wu, L. Wang, H. Zheng, J. F. Mitchell, and C. Leighton, Phys. Rev. B **74**, 134408 (2006).
[8] C. He, M. A. Torija, J. Wu, J. W. Lynn, H. Zheng, J. F. Mitchell, and C. Leighton, Phys. Rev. B **76**, 014401 (2007).
[9] R. H. Potze, G. A. Sawatzky, and M. Abbate, Phys. Rev. B **51**, 11501 (1995).
[10] T. Saitoh, T. Mizokawa, A. Fujimori, M. Abbate, Y. Takeda, and M. Takano, Phys. Rev. B **56**, 1290 (1997).
[11] M. A. Korotin, S. Y. Ezhov, I. V. Solovyev, V. I. Anisimov, D. I. Khomskii, and G. A. Sawatzky, Phys. Rev. B **54**, 5309 (1996).
[12] J. B. Goodenough, Mater. Res. Bull. **6**, 967 (1971).
[13] J. Zaanen, G. A. Sawatzky, and J. W. Allen, Phys. Rev. Lett. **55**, 418 (1985).
[14] D. Louca and J. L. Sarrao, Phys. Rev. Lett. **91**, 155501 (2003).
[15] I. A. Nekrasov, S. V. Streltsov, M. A. Korotin, and V. I. Anisimov, Phys. Rev. B **68**, 235113 (2003).
[16] D. Phelan, D. Louca, K. Kamazawa, S.-H. Lee, S. Rosenkranz, M. F. Hundley, J. F. Mitchell, Y. Motome, S. N. Ancona, and Y. Moritomo, Phys. Rev. Lett. **97**, 235501 (2006).
[17] V. Gnezdilov, V. Fomin, A. V. Yeremenko, K. Y. Choi, Y. Pashkevich, P. Lemmens, S. Shiryaev, G. Bychkov, and S. Barilo, Low Temp. Phys. **32**, 162 (2006).
[18] G. Vanko, J. P. Rueff, A. Mattila, Z. Nemeth, and A. Shukla, Phys. Rev. B **73**, 024424 (2006).
[19] V. P. Plakhty, P. J. Brown, B. Grenier, S. V. Shiryaev, S. N. Barilo, S. V. Gavrilov, and E. Ressouche, J. Phys.: Condens. Matter **18**, 3517 (2006).
[20] R. F. Klie, J. C. Zheng, Y. Zhu, M. Varela, J. Wu, and C. Leighton, Phys. Rev. Lett. **99**, 047203 (2007).
[21] S. K. Pandey, A. Kumar, S. Patil, V. R. R. Medicherla, R. S. Singh, K. Maiti, D. Prabhakaran, A. T. Boothroyd, and A. V. Pimpale, Phys. Rev. B **77**, 045123 (2008).
[22] K. Knizek, Z. Jirak, J. Hejtmanek, and P. Novak, J. Phys.: Condens. Matter **18**, 3285 (2006).
[23] R. J. Radwanski and Z. Ropka, Solid State Commun. **112**, 621 (1999).
[24] R. J. Radwanski and Z. Ropka, Physica B **281-282**, 507 (2000).
[25] Z. Ropka and R. J. Radwanski, Phys. Rev. B **67**, 172401 (2003).
[26] A. Podlesnyak, S. Streule, J. Mesot, M. Medarde, E. Pomjakushina, K. Conder, A. Tanaka, M. W. Haverkort, and D. I. Khomskii, Phys. Rev. Lett. **97**, 247208 (2006).
[27] M. W. Haverkort, Z. Hu, J. C. Cezar, T. Burnus, H. Hartmann, M. Reuther, C. Zobel, T. Lorenz, A. Tanaka, N. B. Brookes, H. H. Hsieh, H.-J. Lin, C. T. Chen, and L. H. Tjeng, Phys. Rev. Lett. **97**, 176405 (2006).
[28] S. Noguchi, S. Kawamata, K. Okuda, H. Nojiri, and M. Motokawa, Phys. Rev. B **66**, 094404 (2002).
[29] M. Medarde, C. Dallera, M. Grioni, J. Voigt, A. Podlesnyak, E. Pomjakushina, K. Conder, T. Neisius, O. Tjenberg, and S. N. Barilo, Phys. Rev. B **73**, 054424 (2006).
[30] H. Hsu, K. Umemoto, M. Cococcioni, and R. Wentzcovitch, Phys. Rev. B **79**, 125124 (2009).
[31] L. Downward, F. Bridges, S. Bushart, J. Neumeier, N. Dilley, and L. Zhou, Phys. Rev. Lett. **95**, 106401 (2005).
[32] Y. Jiang, F. Bridges, L. Downward, and J. J. Neumeier, Phys. Rev. B **76**, 224428 (2007).
[33] E. S. Bozin, M. Schmidt, A. J. DeConinck, G. Paglia, J. F. Mitchell, T. Chatterji, P. G. Radaelli, T. Proffen, and S. J. L. Billinge, Phys. Rev. Lett. **98**, 137203 (2007).
[34] D. Louca, T. Egami, E. L. Brosha, H. Röder, and A. R. Bishop, Phys. Rev. B **56**, R8475 (1997).
[35] N. Sundaram, Y. Jiang, I. E. Anderson, D. P. Belanger, C. H. Booth, F. Bridges, J. F. Mitchell, T. Proffen, and H. Zheng, Phys. Rev. Lett. **102**, 026401 (2009).
[36] N. Sundaram and D. Belanger, (unpublished).
[37] C. H. Booth, R-SPACE X-RAY ABSORPTION PACKAGE, http://lise.lbl.gov/RSXAP/.
[38] F. Bridges, C. H. Booth, M. Anderson, G. H. Kwei, J. J. Neumeier, J. Snyder, J. Mitchell, J. S. Gardner, and E. Brosha, Phys. Rev. B **63**, 214405 (2001).
[39] M. Sikora, C. Kapusta, K. Knizek, Z. Jirak, C. Autret, M. Borowiec, C. J. Oates, V. Prochazka, D. Rybicki, and D. Zajac, Phys. Rev. B **73**, 094426 (2006).
[40] A. R. Han, S. Hwang, Y. Zhao, and Y. Kwon, J. Magn. Magn. Mater. **320**, 1591 (2008).
[41] V. V. Poltavets, M. Croft, and M. Greenblatt, Phys. Rev. B **74**, 125103 (2006).
[42] O. Toulemonde, N. N'Guyen, and F. S. A. Traverse, J. Solid State Chem. **158**, 208 (2001).
[43] D. Phelan, D. Louca, K. Kamazawa, M. F. Hundley, and K. Yamada, Phys. Rev. B **76**, 104111 (2007).
[44] A. N. Petrov, O. F. Kononchuk, A. V. Andreev, V. A. Cherepanov, and P. Kofstad, Solid State Ionics **80**, 189 (1995).
[45] V. V. Sikolenko, A. P. Sazonov, V. V. Efimov, E. A. Efimova, V. V. Kriventsov, D. I. Kochubei, and U. Zimmermann, Crystallogr. Rep. **51**, S67 (2006).
[46] T. Hanashima, N. Shimizu, K. Yamawaki, and S. Sasaki, Jpn. J. Appl. Phys. **46**, 988 (2007).

[47] I. S. Elfimov, V. I. Anisimov, and G. A. Sawatzky, Phys. Rev. Lett. **82**, 4264 (1999).
[48] M. Benfatto, Y. Joly, and C. R. Natoli, Phys. Rev. Lett. **83**, 636 (1999).
[49] G. Thornton, I. W. Owen, and G. P. Diakun, J. Phys.: Condens. Matter **3**, 417 (1991).
[50] J. Y. Chang, B. N. Lin, Y. Y. Hsu, and H. C. Ku, Physica B **329-333**, 826 (2003).
[51] O. Haas, R. P. W. J. Struis, and J. M. McBree, J. Solid State Chem. **177**, 1000 (2004).
[52] T. Hanashima, S. Azuhata, K. Yamawaki, N. Shimizu, and T. Mori, Jpn. J. Appl. Phys. **43**, 4171 (2004).
[53] J. E. Sunstrom IV, K. V. Ramanujachary, M. Greenblatt, and M. Croft, J. Solid State Chem. **139**, 388 (1998).
[54] I. D. Brown, in *Structure and Bonding in Crystals*, edited by M. O'Keeffe and A. Navrotsky (Academic Press, New York, 1981), Vol. 2.
[55] I. D. Brown and D. Altermatt, Acta Crystallogr., Sect. B: Struct. Sci. **41**, 244 (1985).
[56] R. Caciuffo, D. Rinaldi, G. Barucca, J. Mira, J. Rivas, M. A. Senaris-Rodriguez, P. G. Radaelli, D. Fiorani, and J. B. Goodenough, Phys. Rev. B **59**, 1068 (1999).
[57] A. Mineshige, M. Inaba, T. Yao, Z. Ogumi, K. Kikuchi, and M. Kawase, J. Solid State Chem. **121**, 423 (1996).
[58] A. Mineshige, M. Kobune, S. Fujii, Z. Ogumi, M. Inaba, T. Yao, and K. Kikuchi, J. Solid State Chem. **142**, 374 (1999).
[59] G. Vanko, F. de Groot, S. Huotari, R. Cava, T. Lorenz, and M. Reuther, arXiv:0802.2744 (unpublished).
[60] F. Bridges, C. H. Booth, G. H. Kwei, J. J. Neumeier, and G. A. Sawatzky, Phys. Rev. B **61**, R9237 (2000).
[61] G. Thornton, B. C. Tofield, and A. W. Hewat, J. Solid State Chem. **61**, 301 (1986).
[62] A. L. Ankudinov, B. Ravel, J. J. Rehr, and S. D. Conradson, Phys. Rev. B **58**, 7565 (1998).
[63] P. G. Radaelli and S. W. Cheong, Phys. Rev. B **66**, 094408 (2002).
[64] N. W. Ashcroft and N. D. Mermim, *Solid State Physics* (Saunders College, Philadelphia, 1976).
[65] P. A. Lee and G. Beni, Phys. Rev. B **15**, 2862 (1977).
[66] B. K. Teo, *EXAFS: Basic Principles and Data Analysis* (Springer-Verlag, New York, 1986).
[67] A. Bianconi, in *X-ray Absorption: Principles, Applications, Techniques of EXAFS, SEXAFS and XANES*, edited by D. C. Koningsberger and R. Prins (Wiley, New York, 1988), p. 594.
[68] P. Norby, I. G. Krogh Andersen, E. Krogh Andersen, and N. H. Andersen, J. Solid State Chem. **119**, 191 (1995).
[69] D. Louca, J. L. Sarrao, J. D. Thompson, H. Röder, and G. H. Kwei, Phys. Rev. B **60**, 10378 (1999).
[70] G. Maris, Y. Ren, V. Volotchaev, C. Zobel, T. Lorenz, and T. T. M. Palstra, Phys. Rev. B **67**, 224423 (2003).
[71] C. H. Booth, F. Bridges, G. H. Kwei, J. M. Lawrence, A. L. Cornelius, and J. J. Neumeier, Phys. Rev. Lett. **80**, 853 (1998).